

# Drastic Solid-State Fluorescence Enhancement Behaviour of Phenanthro[9,10-*d*]imidazole-Type Fluorescent Hosts upon Inclusion of Carboxylic Acids

Yousuke Ooyama,<sup>\*,[a]</sup> Kazuki Uwada,<sup>[a]</sup> Hironori Kumaoka,<sup>[a]</sup> and Katsuhira Yoshida<sup>\*,[a]</sup>

**Keywords:** Dyes/Pigments / Clathrates / Carboxylic acids / Structure elucidation / Fluorescence

The crystals of phenanthro[9,10-*d*]imidazole-type fluorescent host **1** exhibit drastic fluorescence enhancement behaviour with a redshift in the emission maximum upon enclathration of various carboxylic acids such as formic acid, acetic acid and propionic acid. The optical changes are greatly dependent on the identity of the enclathrated carboxylic acids. The fluorescent clathrate compounds are formed not only by cocrystallization from carboxylic acid solutions but also by solid (fluorescent host)–gas (carboxylic acid vapour) contact. Furthermore, when the acetic acid inclusion crystals are exposed to propionic acid vapour, acetic acid is gradually replaced by propionic acid. The guest exchange of the inclusion crystals was accompanied with colour and fluores-

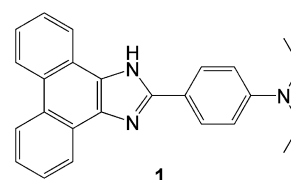
cent intensity changes. The X-ray structural analyses of the guest-free and carboxylic acid inclusion compounds demonstrated that the destructions of the  $\pi$ – $\pi$  interactions, and the intermolecular hydrogen bonds binding fluorophores were induced by the enclathrated carboxylic acid molecules. Moreover, the imidazole ring of the host is protonated by the enclathrated carboxylic acid proton. On the basis of the spectroscopic data and the crystal structures, the effects of the enclathrated carboxylic acid on the solid-state photophysical properties of the clathrate compounds are discussed.

(© Wiley-VCH Verlag GmbH & Co. KGaA, 69451 Weinheim, Germany, 2009)

## Introduction

Solid-state fluorescent organic hosts are attractive materials in the fundamental research field of solid-state photochemistry and in the applied field of optoelectronic devices, because the organic fluorescent host can be the most promising material for the construction of desirable solid-state fluorescent systems.<sup>[1–4]</sup> Several types of fluorescent hosts exhibit fluorescence enhancement behaviour with a blueshift in the fluorescence wavelength maximum upon inclusion of various organic solvent molecules.<sup>[5–11]</sup> From comparison of the X-ray crystal structures of the guest-free and several clathrate compounds, it was concluded that the changes in molecular arrangement by the formation of CH– $\pi$  interactions and the destructions of  $\pi$ – $\pi$  interactions and the intermolecular hydrogen bonds binding fluorophores by the enclathrated guest molecules are the main reason for the guest-dependent fluorescence enhancement and the blueshift in the fluorescence maximum of the crystals. In contrast, we reported that a new phenanthro[9,10-*d*]imidazole-type fluorescent host,<sup>[12]</sup> 2-[4-(diethylamino)phenyl]-1*H*-phenanthro[9,10-*d*]imidazole (**1**; Scheme 1), whose crys-

tals exhibit guest-dependent fluorescence enhancement with a redshift in the emission maximum upon contact with gaseous carboxylic acids such as formic acid, acetic acid and propionic acid.<sup>[11]</sup> Recently, we found that when the acetic acid inclusion crystals are exposed to propionic acid vapour, acetic acid is gradually replaced by propionic acid. The guest exchange of the inclusion crystals were accompanied by colour and fluorescent intensity changes. Furthermore, the fluorescent clathrate compounds are formed by cocrystallization from various carboxylic acid solutions, and the degree of fluorescence enhancement and the redshift in the emission maximum are greatly dependent on the identity of the enclathrated carboxylic acids. In this paper, the effects of enclathrated carboxylic acids on the solid-state photophysical properties and crystal-packing structures of **1** are discussed on the basis of the X-ray crystal structures of the guest-free and carboxylic acid inclusion compounds.



Scheme 1. Chemical structure of phenanthro[9,10-*d*]imidazole-type fluorescent clathrate host **1**.

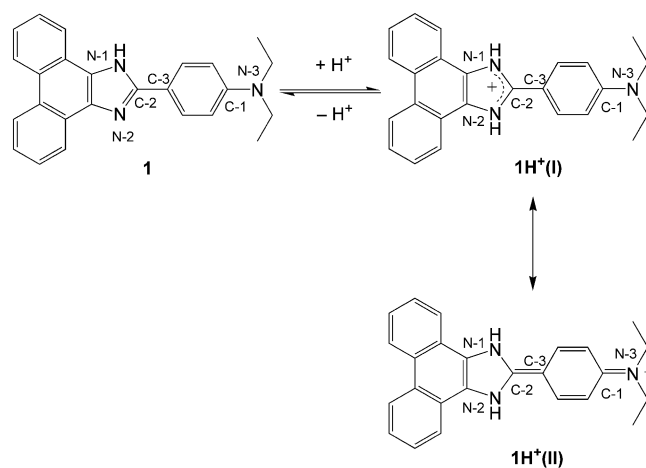
[a] Department of Material Science, Faculty of Science, Kochi University  
Akebono-cho, Kochi 780-8520, Japan  
Fax: +81-88-844-8359  
E-mail: yooyama@hiroshima-u.ac.jp  
kyoshida@cc.kochi-u.ac.jp

## Results and Discussion

Spectroscopic Properties of **1** in Solution

The absorption and fluorescence spectroscopic data of **1** in 1,4-dioxane, ethanol and acetic acid summarized in Table 1 and the spectra of **1** are shown in Figure 1. Fluorophore **1** exhibits an absorption band at around 347 nm and a fluorescence band at around 408 nm in 1,4-dioxane. In contrast, in ethanol, fluorophore **1** exhibits an absorption band at around 341 nm with a shoulder at 371 nm and a fluorescence band at around 419 nm. Interestingly, in acetic acid, the absorption and fluorescence bands of **1** appear at around 376 and 423 nm, respectively, which are redshifted by 29 and 15 nm, respectively, relative to those observed in 1,4-dioxane. Dogra et al. reported that the absorption and

fluorescence maxima of 2-[4'-(*N,N*-dimethylamino)phenyl]-benzimidazole in acidic solution are redshifted relative to those in neutral solution.<sup>[13]</sup> They demonstrated that the redshifts are induced by protonation of an imino nitrogen atom of the imidazole ring. Therefore, it is suggested that the observed redshifts of **1** in acetic acid are caused by protonation of an imino nitrogen atom of the imidazole ring, as shown in Scheme 2. The fluorescence quantum yield ( $\Phi$ ) of **1** in 1,4-dioxane, ethanol and acetic acid are 0.56, 0.52 and 0.68, respectively.

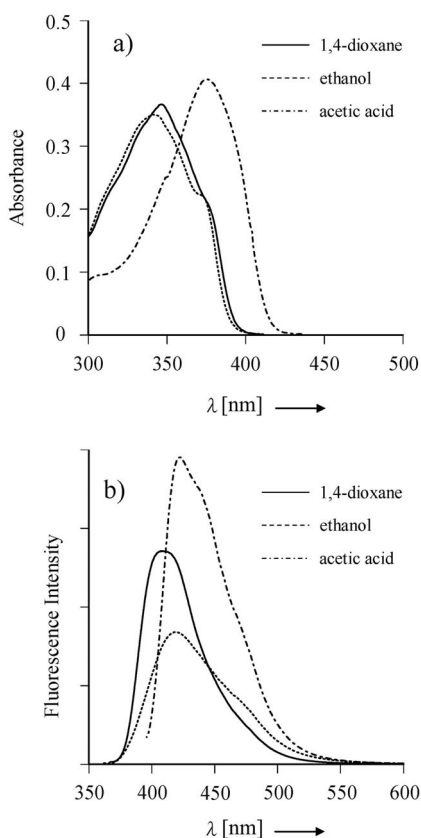


Scheme 2.

Table 1. Spectroscopic properties of **1** in solution.

Solvent	$\lambda_{\max}^{\text{abs}}$ [nm] <sup>[a]</sup> ( $\epsilon_{\max}$ [dm <sup>3</sup> mol <sup>-1</sup> cm <sup>-1</sup> ])	$\lambda_{\max}^{\text{fl}}$ [nm] <sup>[b]</sup>	$\Phi$ <sup>[c]</sup>	SS <sup>[d]</sup> $\Delta\lambda_{\max}$
1,4-Dioxane	347 (36700)	408	0.56	61
Ethanol	341 (35100), 372 (22200)	419	0.52	78
Acetic acid	376 (40600)	423	0.68	47

[a]  $1.0 \times 10^{-5}$  M. [b]  $1.0 \times 10^{-6}$  M. [c] The  $\Phi$  values were determined by using a calibrated integrating sphere system ( $\lambda_{\text{ex}} = 363$  nm). [d] Stokes shift value.

Figure 1. (a) Absorption and (b) fluorescence spectra of **1** in 1,4-dioxane, ethanol and acetic acid.

## Semiempirical MO Calculations (AM1, CNDO/S)

To understand the photophysical properties of 2-[4-(diethylamino)phenyl]-1*H*-phenanthro[9,10-*d*]imidazole (**1**), we carried out semiempirical molecular orbital (MO) calculations of **1** by the CNDO/S method<sup>[14]</sup> after geometrical optimization by the MOPAC/AM1 method.<sup>[15]</sup> Furthermore, we estimated the photophysical properties for **1H**<sup>+</sup> with the protonated imidazole ring, because it was assumed that the imino nitrogen atom of the imidazole ring is protonated in acidic solution. As shown in Figure 2, the optimized geometry of **1** shows that the bond lengths between the N-1 and N-2 nitrogen atoms and C-2 in the imidazole ring are 1.41 and 1.36 Å, respectively. This result shows that the differences between the two lengths for **1** are attributed to the C–N and C=N bonds of the imidazole ring. In contrast, the two bond lengths for **1H**<sup>+</sup> with the protonated imidazole ring are both 1.39 Å, which reveals the contribution of the resonance structure **1H**<sup>+</sup>(I), as shown in Scheme 2. In contrast, the bond lengths between C-3 of the phenyl group and C-2 in the imidazole ring are 1.46 Å for **1** and 1.44 Å for **1H**<sup>+</sup>, and the bond lengths between C-1 of the phenyl group and N3 of the diethylamino group are 1.40 Å for **1** and 1.37 Å for **1H**<sup>+</sup>. The two bond lengths of **1H**<sup>+</sup> are shorter than those of **1**, which indicates the contribution of the resonance structure **1H**<sup>+</sup>(II), as shown in Scheme 2. The calculated absorption wavelengths and the

nature of the transition of the first absorption bands are collected in Table 2. The calculated absorption wavelengths and the oscillator strength values of **1** and **1H<sup>+</sup>** are comparable with the observed spectra in 1,4-dioxane and acetic acid; the calculated absorption wavelength of **1H<sup>+</sup>** is shifted to longer wavelength relative to that of **1**, which is in good agreement with the experimental data in 1,4-dioxane and acetic acid. Therefore, the redshift of **1** in acetic acid was explained by the resonance interaction of the diethylamino group with the imidazole ring, leading to a resonance hybrid of **1H<sup>+</sup>(I)** and **1H<sup>+</sup>(II)**.

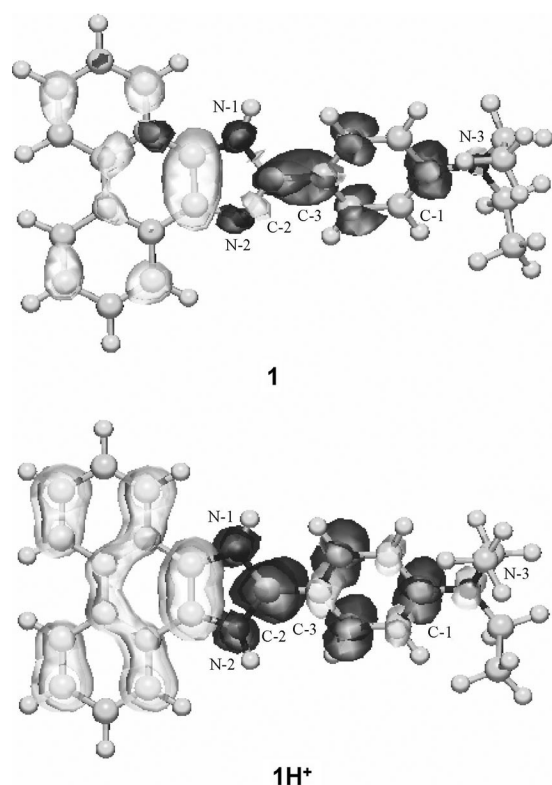


Figure 2. Calculated electron density changes accompanying the first electronic excitation of **1** and **1H<sup>+</sup>**. The black and white lobes signify decreases and increase in electron density accompanying the electronic transition. Their areas indicate the magnitude of the electron density change.

Table 2. Calculated absorption spectra for **1** and **1H<sup>+</sup>**.

Species	$\mu$ [D] <sup>[a]</sup>	Absorption (calcd.) $\lambda_{\text{max}}$ [nm]	$f^{\text{[b]}}$	CI component <sup>[c]</sup>	$\Delta\mu$ [D] <sup>[d]</sup>
<b>1</b>	4.55	371	0.67	HOMO→LUMO (75%)	2.66
<b>1H<sup>+</sup></b>	2.12	446	0.70	HOMO→LUMO (90%)	8.43

[a] Values of the dipole moment in the ground state. [b] Oscillator strength. [c] The transition is shown by an arrow from one orbital to another, followed by its percentage CI (configuration interaction) component. [d] The values of the difference in the dipole moment between the excited and ground states.

## Fluorescence Sensing Behaviour of Crystals of **1** upon Contact with Gaseous Carboxylic Acids

Recrystallization of **1** from acetonitrile gave needle-shaped crystals that contain no solvent molecules. Interestingly, when the guest-free crystals were placed in a vessel saturated with carboxylic acid vapour at 30 °C, the colour of the crystals turned from colourless to yellow. By solid-state fluorescence measurement, we found that a redshift in the excitation and emission maxima and a guest-dependent fluorescence enhancement are induced upon inclusion of the guest molecules. As an example, the fluorescence excitation and emission spectral changes in the guest-free crystals of **1** upon exposure to acetic acid vapour are shown in Figure 3, and Table 3 summarizes the time-dependent changes in the excitation and emission spectra of the guest-free crystals upon exposure to gaseous formic acid, acetic acid and propionic acid, respectively. At the time intervals, a small portion of the exposed crystals was withdrawn and checked by <sup>1</sup>H NMR spectroscopy, which demonstrated that carboxylic acid molecules are gradually included into the crystals, and clathrate formation by solid–gas contact is suggested. The maximum fluorescence was obtained when the host-to-guest stoichiometric ratio attained was near 1:2 in every case. The initial excitation band at 378 nm of the guest-free crystals was shifted to 447 nm for **1**·formic acid (1:2), 442 nm for **1**·acetic acid (1:2) and 443 nm for **1**·propionic acid (1:2). The corresponding fluorescence spectra showed an increase in the fluorescence intensity with a redshift in the emission maximum from 468 to 474 nm for **1**·formic acid (1:2), 473 nm for **1**·acetic acid (1:2), and 511 nm for **1**·propionic acid (1:2). The maximum fluorescence intensities of the guest-inclusion crystals after exposure to gaseous formic acid, acetic acid and propionic acid were about 5-, 33- and 50-fold stronger than the fluorescence intensity of the starting guest-free crystals, respectively. Moreover, continuous exposure of the crystals resulted in further inclusion of carboxylic acid molecules until the host-to-guest stoichiometric ratio was 1:3, and the fluorescence intensity decreased slightly in every case. It took about 150 min for **1**·formic acid (1:3), 900 min for **1**·acetic acid (1:3), and 2400 min for **1**·propionic acid (1:3). These results suggest that increasing the molecular size of the enclathrated carboxylic acid tends to induce a larger fluorescence enhancement, but it also slows down the formation of the clathrate.

More interestingly, when the above-mentioned powders of **1**·acetic acid (1:3) and **1**·propionic acid (1:3) were exposed to propionic acid and acetic acid vapour, respectively, exchange of the guest molecules was observed. Guest molecules of acetic acid and propionic acid were gradually replaced by propionic acid and acetic acid, respectively. In the above case, the former guest molecules were completely removed when the ratio of the host to the latter guest reached 1:2 after about 10–20 min. Continuous exposure of the crystals resulted in further inclusion of carboxylic acid molecules until the host to the latter guest stoichiometric ratio became 1:3. The guest exchange of the inclusion crys-

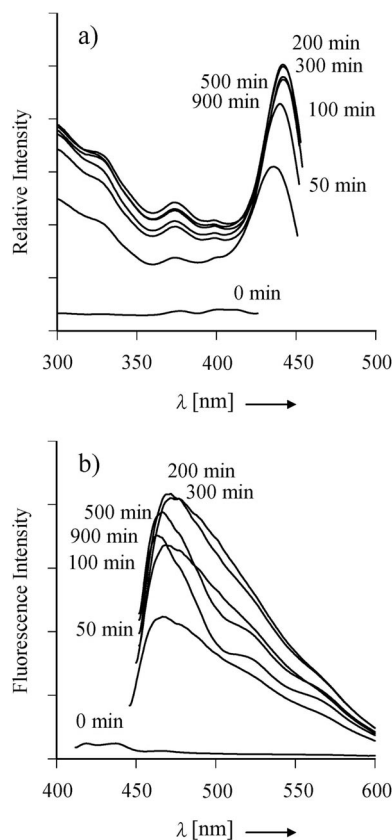


Figure 3. Time-dependent spectral changes of the guest-free crystals of **1** upon exposure to acetic acid vapour at 30 °C; (a) the excitation and (b) emission spectra were recorded at their corresponding emission and excitation maxima.

Table 3. Time-dependent changes in the excitation and emission wavelength, fluorescence intensity and host-to-guest ratios of the guest-free crystals of **1** upon contact with gaseous carboxylic acids at 30 °C.

Guest acid	Time [min]	Excitation $\lambda_{\text{ex}}$ [nm]	Emission $\lambda_{\text{em}}$ [nm]	RFI <sup>[a]</sup>	Ratio <sup>[b]</sup> host/guest
Formic acid	0	378	468	1.00	1:0
	10	445	473	4.61	1:0.6
	20	446	474	5.05	1:1.2
	50	447	474	5.14	1:2.2
	150	448	474	4.42	1:2.9
Acetic acid	0	378	468	1.00	1:0
	50	436	468	17.9	1:0.5
	100	440	471	26.9	1:1.1
	200	442	474	32.8	1:1.9
	300	442	473	33.4	1:2.3
	900	442	464	28.1	1:3.0
Propionic acid	0	378	468	1.00	1:0
	120	441	511	35.2	1:0.3
	300	443	511	43.4	1:1.1
	420	443	511	50.8	1:2.0
	1200	443	513	50.4	1:2.9
	2400	443	513	49.6	1:3.0

[a] Relative fluorescence intensity was determined by considering the fluorescence intensity of the guest-free crystal of **1** as 1.0. [b] Determined by integration of the signals in the <sup>1</sup>H NMR spectra.

tals was accompanied by colour and fluorescent intensity changes. When the powders of **1**·acetic acid (1:3) were exposed to propionic acid vapour, a redshift in the excitation and emission maxima and a fluorescence enhancement were induced upon exchange of acetic acid with propionic acid (Figure 4a). In contrast, when the powders of **1**·propionic acid (1:3) were exposed to acetic acid, a blueshift in the excitation and emission maxima and a slight change in fluorescence intensity were induced upon exchange of propionic acid with acetic acid (Figure 4b). Table 4 summarizes the time-dependent changes in the excitation and emission spectra upon exchange of acetic acid with propionic acid and upon exchange of propionic acid with acetic acid, respectively. It is worth noting that the excitation and fluorescence wavelength maxima of **1**·acetic acid (1:2) and **1**·propionic acid (1:2), which were prepared by exchange of guest molecules, are slightly different from those of **1**·acetic acid (1:2) and **1**·propionic acid (1:2) prepared by guest-free crystals/carboxylic acid vapour contact (Table 3). These results indicate that the photophysical spectral changes upon solid–gas contact reflect strictly the changes in molecular packing induced by the enclathrated guest molecules in the crystals, and there are slight differences in the degree of changes in molecular packing between the guest-free crystals/carboxylic acid vapour contact and the exchange of guest molecules.

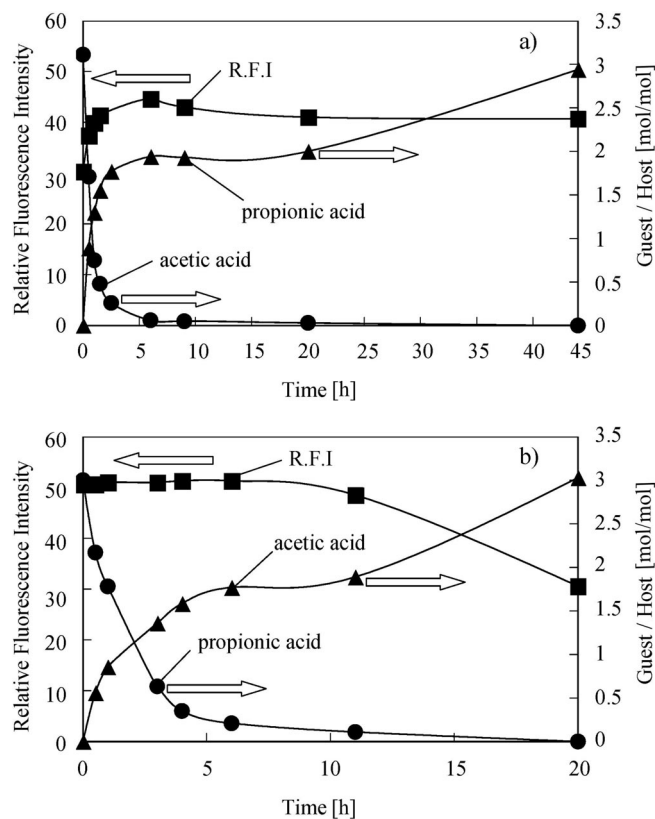


Figure 4. Time-dependent changes in the fluorescence intensity upon guest exchange by gas–solid contact at 30 °C; (a) **1**·acetic acid (1:3) exposed to propionic vapour and (b) **1**·propionic acid (1:3) exposed to acetic acid vapour.

Table 4. Time-dependent changes in the excitation and emission wavelength, fluorescence intensity and host-to-guest ratios upon guest exchange by solid–gas contact at 30 °C; **1**·acetic acid (1:3) was exposed to propionic vapour and **1**·propionic acid (1:3) was exposed to acetic acid vapour.

Guest exchange	Time [h]	Excitation $\lambda_{\text{ex}}$ [nm]	Emission $\lambda_{\text{em}}$ [nm]	RFI <sup>[a]</sup>	Ratio <sup>[b]</sup> host/acetic acid/propionic acid	
Acetic acid →	0	442	463	30.3	1:3:0	
	0.5	438	489	37.4	1:1.71:0.89	
	1	438	491	39.9	1:0.75:1.30	
	Propionic acid	1.5	438	491	41.4	1:0.48:1.55
		6	437	492	44.6	1:0.06:1.94
9		437	492	43.0	1:0.05:1.95	
Propionic acid →	20	437	493	41.0	1:0.03:2.00	
	44	438	507	40.7	1:0.2.94	
	0	443	513	50.6	1:0:3	
	0.5	443	513	50.6	1:0.56:2.17	
	1	442	508	41.0	1:0.86:1.78	
Acetic acid	3	438	483	51.0	1:1.36:0.63	
	4	436	478	51.3	1:1.59:0.35	
	6	436	477	51.3	1:1.77:0.21	
	11	436	473	48.5	1:1.89:0.11	
	20	438	462	30.6	1:3:0	

[a] Relative fluorescence intensity was determined by considering the fluorescence intensity of the guest-free crystals of **1** as 1.0. [b] Determined by integration of the signals in the <sup>1</sup>H NMR spectra.

### Solid-State Fluorescence Properties of the Clathrate Compounds Prepared by Cocrystallization of **1** from Carboxylic Acid Solutions

In order to investigate the carboxylic acid inclusion ability of **1**, we recrystallized fluorophore **1** from various carboxylic acid solutions. We found that fluorophore **1** yields various host–guest inclusion compounds in stoichiometric ratios with carboxylic acids such as formic acid, acetic acid, propionic acid, benzoic acid and sebacic acid in the crystalline state. The characteristics of the guest-free and various carboxylic acid inclusion crystals obtained by cocrystallization

of **1** from carboxylic acid solutions are summarized in Table 5. Interestingly, for formic acid, acetic acid, propionic acid, 2,2-dimethyl-*n*-butyric acid and 3,3-dimethyl-*n*-butyric acid, the host/guest ratio varies depending on the carboxylic acid solutions used as recrystallization solvents. When a mixture of carboxylic acid and acetonitrile was used, the host/guest ratio became 1:2. In contrast, when only carboxylic acid was used, the host/guest ratio became 1:3, except for formic acid. The solution jelled when only formic acid was used. In comparison to the guest-free crystals, the colour of the carboxylic acid inclusion crystals varied from colourless to yellow and a dramatic fluorescence enhancement was observed.

In order to investigate the effect of clathrate formation on the solid-state photophysical properties, the fluorescence excitation and emission spectra of the guest-free and the carboxylic acid inclusion crystals were measured (Figure 5). The solid-state photophysical changes are greatly dependent on the identity of the enclathrated carboxylic acids. In comparison to the guest-free crystal, the excitation and emission maxima of the guest-inclusion crystals exhibited a redshift and the fluorescence intensity was enhanced to various degrees depending on the identity of the enclathrated carboxylic acid molecules. The excitation and fluorescence spectroscopic data of the guest-free and carboxylic acid inclusion crystals are summarized in Table 6. The 428-nm band observed in the excitation spectrum of the guest-free crystals shifted to around 430–451 nm in those of the carboxylic acid inclusion crystals. The guest-free host crystal exhibits relatively weak fluorescence with emission maximum at 468 nm, whereas the carboxylic acid inclusion crystals exhibit much stronger fluorescence intensity with an emission maximum redshifted to around 499–512 nm. In comparison with the guest-free crystal, the fluorescence intensities of the guest-inclusion crystals were ca. 26-fold in **1**·(CH<sub>3</sub>COOH)<sub>2</sub>, ca. 40-fold in **1**·(CH<sub>3</sub>CH<sub>2</sub>COOH)<sub>2</sub>, ca. 56-fold in **1**·[CH<sub>3</sub>CH<sub>2</sub>C(CH<sub>2</sub>)<sub>2</sub>COOH]<sub>2</sub> and ca. 51-fold in **1**·[HOOC(CH<sub>2</sub>)<sub>8</sub>COOH]<sub>2</sub>. It is noteworthy that the excitation and fluorescence wavelength maxima and solid-state

Table 5. Host–guest molar ratio, crystal form and crystal colour of the guest-free and the guest-inclusion crystals of **1**.

Clathrate compound	Host/guest	Guest	Crystal colour	Crystal form	Recrystallization solvent
Guest-free	1:0	none	milk-white	needle	acetonitrile
<b>1</b> ·(HCOOH) <sub>2</sub>	1:2	formic acid	yellow	needle	formic acid/acetonitrile (1:6)
<b>1</b> ·(CH <sub>3</sub> COOH) <sub>2</sub>	1:2	acetic acid	yellow	prism	acetic acid/acetonitrile (1:3)
<b>1</b> ·(CH <sub>3</sub> COOH) <sub>3</sub>	1:3	acetic acid	yellow	prism	acetic acid
<b>1</b> ·(CH <sub>3</sub> CH <sub>2</sub> COOH) <sub>2</sub>	1:2	propionic acid	yellow	prism	propionic acid/acetonitrile (1:1)
<b>1</b> ·(CH <sub>3</sub> CH <sub>2</sub> COOH) <sub>3</sub>	1:3	propionic acid	yellow	prism	propionic acid
<b>1</b> ·[CH <sub>3</sub> (CH <sub>2</sub> ) <sub>4</sub> COOH] <sub>2</sub>	1:2	hexanoic acid	yellow	prism	hexanoic acid/acetonitrile (1:3)
<b>1</b> ·[CH <sub>3</sub> (CH <sub>2</sub> ) <sub>4</sub> COOH] <sub>3</sub>	1:3	hexanoic acid	yellow	prism	hexanoic acid
<b>1</b> ·[(CH <sub>3</sub> ) <sub>2</sub> CCH <sub>2</sub> COOH] <sub>2</sub>	1:2	2,2-dimethyl- <i>n</i> -butyric acid	yellow	needle	2,2-dimethyl- <i>n</i> -butyric acid/acetonitrile (1:1)
<b>1</b> ·[(CH <sub>3</sub> ) <sub>2</sub> CCH <sub>2</sub> COOH] <sub>3</sub>	1:3	2,2-dimethyl- <i>n</i> -butyric acid	yellow	needle	2,2-dimethyl- <i>n</i> -butyric acid
<b>1</b> ·[CH <sub>3</sub> CH <sub>2</sub> C(CH <sub>2</sub> ) <sub>2</sub> COOH] <sub>2</sub>	1:2	3,3-dimethyl- <i>n</i> -butyric acid	yellow	prism	3,3-dimethyl- <i>n</i> -butyric acid/acetonitrile (1:3)
<b>1</b> ·[CH <sub>3</sub> CH <sub>2</sub> C(CH <sub>2</sub> ) <sub>2</sub> COOH] <sub>3</sub>	1:3	3,3-dimethyl- <i>n</i> -butyric acid	yellow	prism	3,3-dimethyl- <i>n</i> -butyric acid
<b>1</b> ·benzoic acid	1:1	benzoic acid	white	needle	acetonitrile solution containing benzoic acid
<b>1</b> · <i>m</i> -dimethylaminobenzoic acid	1:1	<i>m</i> -dimethylaminobenzoic acid	yellow	needle	acetonitrile solution containing <i>m</i> -dimethylaminobenzoic acid
<b>1</b> ·[HOOC(CH <sub>2</sub> ) <sub>2</sub> COOH] <sub>2</sub>	2:1	succinic acid	yellow	prism	acetonitrile solution containing succinic acid
<b>1</b> ·[HOOC(CH <sub>2</sub> ) <sub>8</sub> COOH] <sub>2</sub>	2:1	sebacic acid	yellow	prism	acetonitrile solution containing sebacic acid

fluorescence intensity of the carboxylic acid inclusion crystals prepared by recrystallization are slightly different from those of carboxylic acid inclusion solids prepared by guest-free crystals/ carboxylic acid vapour contact (Table 3).

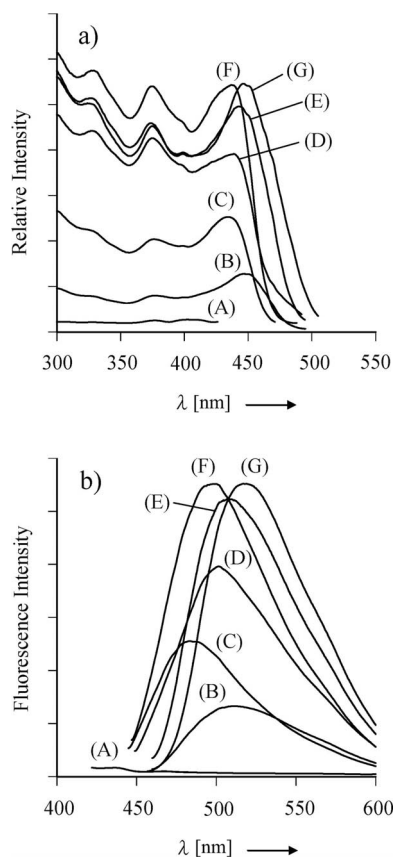


Figure 5. (a) Solid-state excitation and (b) fluorescence spectra of the guest-free and the carboxylic acid inclusion crystals of **1**; (A) **1** (guest-free), (B) **1**·[HOOC(CH<sub>2</sub>)<sub>2</sub>COOH]<sub>2</sub>, (C) **1**·(CH<sub>3</sub>COOH)<sub>2</sub>, (D) **1**·(CH<sub>3</sub>CH<sub>2</sub>COOH)<sub>2</sub>, (E) **1**·[HOOC(CH<sub>2</sub>)<sub>8</sub>COOH]<sub>2</sub>, (F) **1**·[CH<sub>3</sub>CH<sub>2</sub>C(CH<sub>2</sub>)<sub>2</sub>COOH]<sub>2</sub> and (G) **1**·(HCOOH)<sub>2</sub>.

Table 6. Excitation and fluorescence spectroscopic data of the guest free and various carboxylic acid inclusion crystals of **1**.

Clathrate compound	Excitation $\lambda_{\text{ex}}$ [nm]	Emission $\lambda_{\text{em}}$ [nm]	RFI <sup>[a,b]</sup>
Guest-free	378	468	1.0
<b>1</b> ·(HCOOH) <sub>2</sub>	446	519	56.3
<b>1</b> ·(CH <sub>3</sub> COOH) <sub>2</sub>	435	484	26.0
<b>1</b> ·(CH <sub>3</sub> CH <sub>2</sub> COOH) <sub>2</sub>	439	502	40.4
<b>1</b> ·[CH <sub>3</sub> (CH <sub>2</sub> ) <sub>4</sub> COOH] <sub>2</sub>	446	506	44.5
<b>1</b> ·[CH <sub>3</sub> CH <sub>2</sub> C(CH <sub>2</sub> ) <sub>2</sub> COOH] <sub>2</sub>	437	499	56.2
<b>1</b> ·[(CH <sub>3</sub> ) <sub>3</sub> CCH <sub>2</sub> COOH] <sub>2</sub>	447	510	46.4
<b>1</b> ·benzoic acid	451	497	4.5
<b>1</b> · <i>m</i> -dimethylaminobenzoic acid	420	500	28.0
<b>1</b> ·[HOOC(CH <sub>2</sub> ) <sub>2</sub> COOH] <sub>2</sub>	447	513	13.4
<b>1</b> ·[HOOC(CH <sub>2</sub> ) <sub>8</sub> COOH] <sub>2</sub>	444	508	51.2

[a] Relative fluorescence intensity was determined by considering the fluorescence intensity of the guest-free crystal of **1** as 1.0. [b] As the standard sample, the RFI of anthracene crystal ( $\lambda_{\text{ex}} = 370$  nm,  $\lambda_{\text{em}} = 445$  nm) is 42.<sup>[9]</sup>

These results indicate that there are some differences in the molecular packings between the clathrate compounds prepared by cocrystallization and by solid–gas contact.

### Relation between Solid-State Fluorescence Properties and X-ray Crystal Structures of Carboxylic Acid Inclusion Compounds

To investigate the relationship between the observed solid-state fluorescence properties and the changes in molecular packing structure upon inclusion of the guest molecules, the crystal structures of the guest-free crystal of **1** and the carboxylic acid inclusion compounds **1**·(CH<sub>3</sub>COOH)<sub>2</sub>, **1**·(CH<sub>3</sub>CH<sub>2</sub>COOH)<sub>2</sub>, **1**·[CH<sub>3</sub>CH<sub>2</sub>C(CH<sub>2</sub>)<sub>2</sub>COOH]<sub>2</sub> and **1**·[HOOC(CH<sub>2</sub>)<sub>8</sub>COOH]<sub>2</sub> were determined by X-ray diffraction analysis.

In the guest-free crystal, host molecules are linked by intermolecular NH···N hydrogen bonds between the imidazole nitrogen atoms to form a linear molecular chain along the *c* axis (Figure 6a). The host molecules along the chain are related by 4<sub>1</sub> (fourfold screw axis) symmetry, as shown in Figure 6b. The bond lengths between the N-1 and N-2 nitrogen atoms and C-2 in the imidazole ring are 1.39 and 1.30 Å, respectively. The differences between the two lengths for **1** are attributed to the C–N and C=N bonds of the imidazole ring. Between the adjacent chains there are two short molecular contacts between host molecules; one results from the overlapping of the *p*-(diethylamino)phenyl parts (Figure 6c: stacking I) and the other is the  $\pi$ – $\pi$  overlapping of the phenanthrene parts, where there are 11 short interatomic  $\pi$ – $\pi$  contacts of less than 3.6 Å (Figure 6d: stacking II). These long-range host–host interactions based on continuous intermolecular hydrogen bonds and  $\pi$ – $\pi$  interactions would cause a strong fluorescence quenching in the guest-free crystal.<sup>[5–8,11]</sup>

In contrast, in the case of the carboxylic acid inclusion crystals, such direct intermolecular hydrogen bonding between host molecules is not found. Instead, the carboxylic acid inclusion crystals, except those of **1**·[HOOC(CH<sub>2</sub>)<sub>8</sub>COOH]<sub>2</sub>, are made up of a hydrogen-bonded cluster unit composed of two imidazole hosts and four carboxylic acid guests (Figures 7, 8 and 9). The two hosts and two of the four guests are alternately linked by four NH···O hydrogen bonds to form a centrosymmetric ring, in which the imidazole ring is protonated by the carboxylic acid proton (Figures 7b, 8b and 9b). Actually, the two bond lengths between the N(1) and N(2) nitrogen atoms and C(15) in the imidazole ring are ca. 1.34 and ca. 1.35 Å, respectively, which are nearly the same. The other two guests are linked by a hydrogen bond to each of the two ring-forming guests to form a hexamer cluster unit. These results suggest that the imidazole ring effectively fixes carboxylic acid molecules in the crystalline state. There are two styles of  $\pi$ – $\pi$  stacking between host molecules. One is the  $\pi$ – $\pi$  overlapping between the phenanthroimidazole and *p*-(diethylamino)phenyl parts in the cluster unit (Figures 7c, 8c and 9c: stacking I). For **1**·(CH<sub>3</sub>COOH)<sub>2</sub>, **1**·(CH<sub>3</sub>CH<sub>2</sub>COOH)<sub>2</sub> and **1**·[CH<sub>3</sub>–

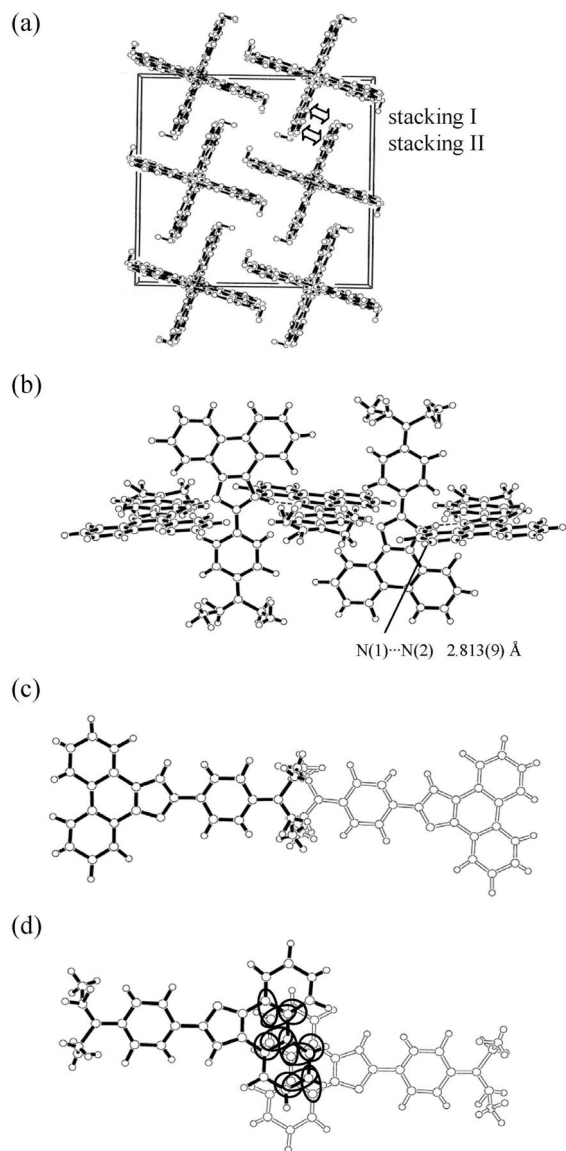


Figure 6. Crystal structure of **1**: (a) a stereoview of the molecular packing structure, (b) intermolecular hydrogen bonds between the fluorophores, (c) top view of a cluster unit (stacking I) and (d) a top view between two cluster units (stacking II). The dotted lines in (b) indicate hydrogen bonds. The circles represented in (d) show short interatomic  $\pi$ - $\pi$  contacts of less than 3.6 Å.

$\text{CH}_2\text{C}(\text{CH}_2)_2\text{COOH}]_2$ , there are 9, 23 and 23 short interatomic  $\pi$ - $\pi$  contacts of less than 3.6 Å, and the average distances of the interatomic  $\pi$ - $\pi$  contacts are ca. 3.39, ca. 3.49 and ca. 3.47 Å, respectively. The other is observed between the neighbouring cluster units, where the phenanthrene ring parts are overlapping (Figures 7d, 8d and 9d: stacking II). There are 32, 22 and 7 short interatomic  $\pi$ - $\pi$  contacts of less than 3.6 Å, and the average distances of the interatomic  $\pi$ - $\pi$  contacts are ca. 3.50, ca. 3.51 and ca. 3.53 Å, respectively. In contrast, the crystal of **1**·[HOOC(CH<sub>2</sub>)<sub>8</sub>COOH]<sub>2</sub> is made up of a hydrogen-bonded cluster unit composed of two hosts and two sebacic acid guests (Figure 10). Although the two hosts and two guests

are alternately linked by four NH...O hydrogen bonds to form a centrosymmetric ring, in which the imidazole ring is protonated by the sebacic acid proton [N(1)-C(15) ca. 1.34 Å and N(2)-C(15) ca. 1.35 Å], interestingly the neighbouring cluster units are connected through two carboxyl

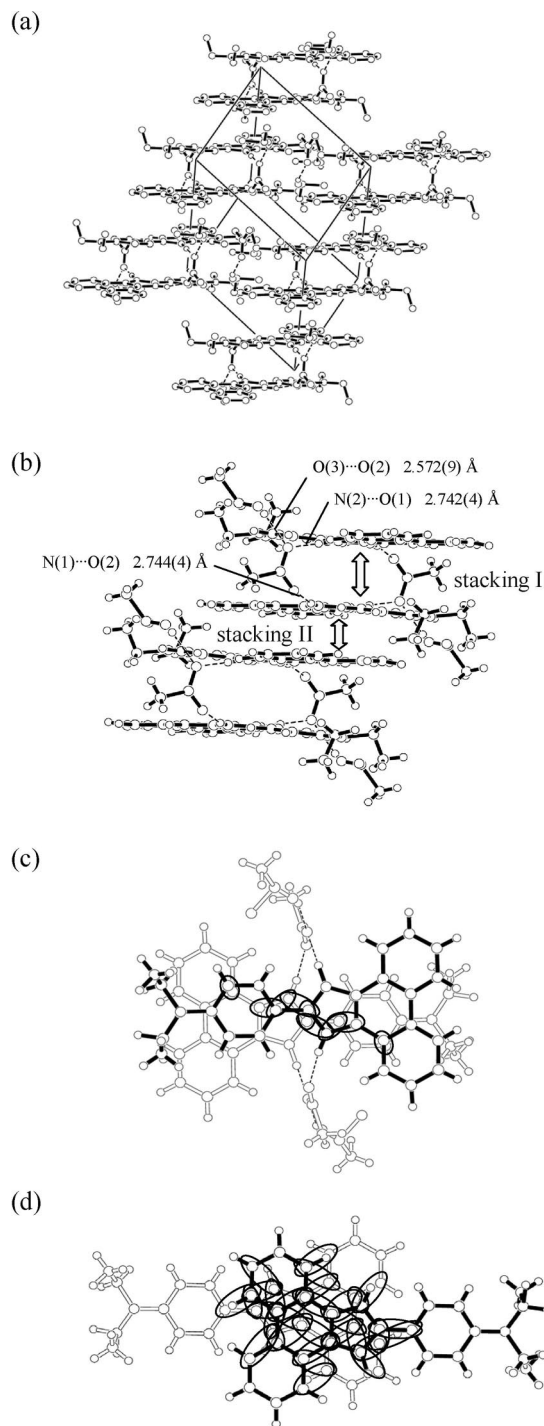


Figure 7. Crystal structure of **1**·(CH<sub>3</sub>COOH)<sub>2</sub>: (a) a stereoview of the molecular packing structure, (b) intermolecular hydrogen bonds, (c) top view of a cluster unit (stacking I) and (d) a top view between two cluster units (stacking II). The dotted lines in (b) indicate hydrogen bonds. The circles represented in (c) and (d) show short interatomic  $\pi$ - $\pi$  contacts of less than 3.6 Å.

groups on both sides of the sebacic acid. Therefore, a continuous intermolecular hydrogen-bonding chain of ( $\cdots\text{H}\cdots\text{G}\cdots\text{H}\cdots$ ) is formed through the above intermolecular hydrogen bonding ( $\text{NH}\cdots\text{O}$ ) between hosts and sebacic acid molecules. The  $\pi$ - $\pi$  overlapping between the phenan-

throidiazole and *p*-(diethylamino)phenyl parts in the cluster unit was observed, and there are 23 short interatomic  $\pi$ - $\pi$  contacts of less than 3.6 Å, and the average distance of

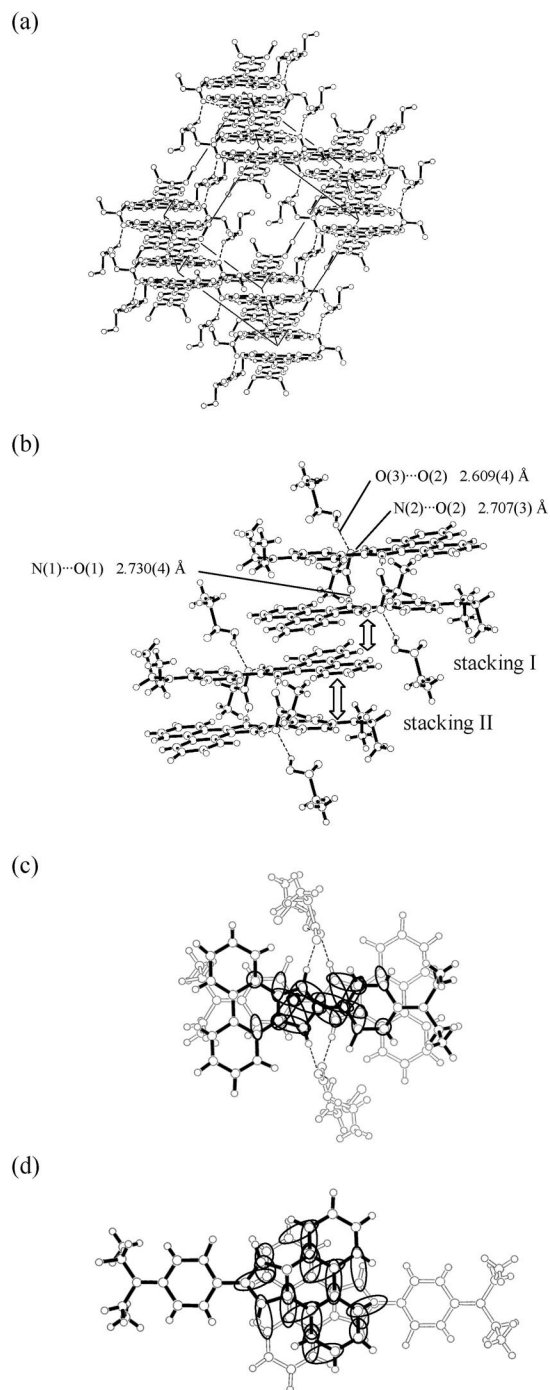


Figure 8. Crystal structure of  $1\cdot(\text{CH}_3\text{CH}_2\text{COOH})_2$ : (a) a stereoview of the molecular packing structure, (b) intermolecular hydrogen bonds, (c) top view of a cluster unit (stacking I) and (d) a top view between two cluster units (stacking II). The dotted lines in (b) indicate hydrogen bonds. The circles represented in (c) and (d) show short interatomic  $\pi$ - $\pi$  contacts of less than 3.6 Å.

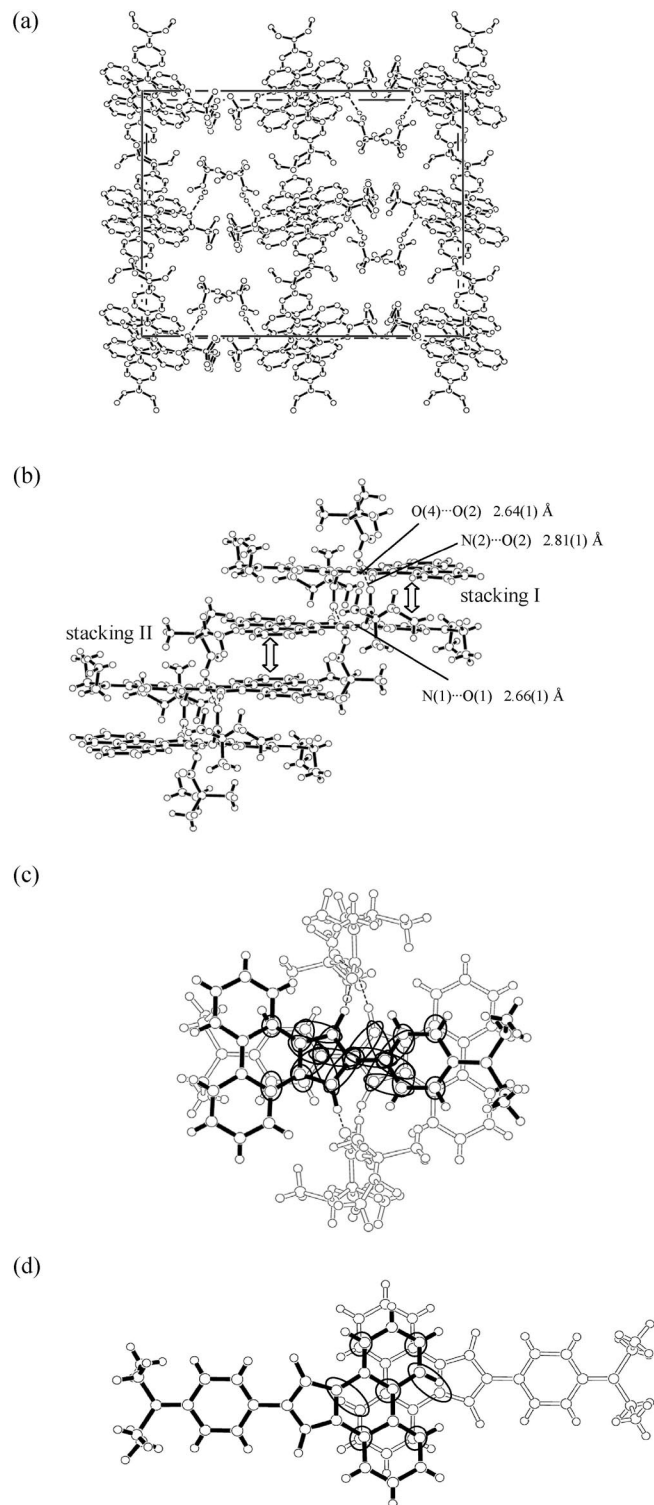


Figure 9. Crystal structure of  $1\cdot[\text{CH}_3\text{CH}_2\text{C}(\text{CH}_2)_2\text{COOH}]_2$ : (a) a stereoview of the molecular packing structure, (b) intermolecular hydrogen bonds, (c) top view of a cluster unit (stacking I) and (d) a top view between two cluster units (stacking II). The dotted lines in (b) indicate hydrogen bonds. The circles represented in (c) and (d) show short interatomic  $\pi$ - $\pi$  contacts of less than 3.6 Å.

the interatomic  $\pi$ - $\pi$  contacts is ca. 3.45 Å. However, the  $\pi$ - $\pi$  overlapping of two hosts between the neighbouring cluster units was not observed.

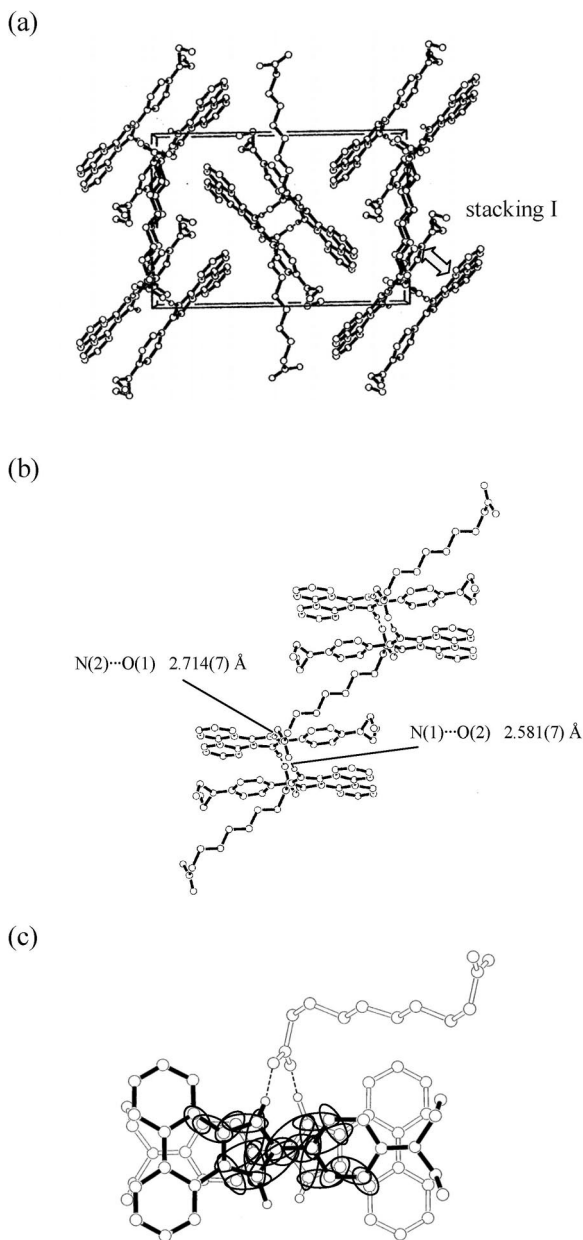


Figure 10. Crystal structure of  $1 \cdot [\text{HOOC}(\text{CH}_2)_8\text{COOH}]_2$ : (a) a stereoview of the molecular packing structure, (b) intermolecular hydrogen bonds and (c) top view of a cluster unit (stacking I). The dotted lines in (b) indicate hydrogen bonds. The circles represented in (c) show short interatomic  $\pi$ - $\pi$  contacts of less than 3.6 Å.

On the basis of the solid-state photophysical data and the crystal structures of the guest-free and carboxylic acid inclusion compounds, we discuss the effects of the enclathrated carboxylic acid on the solid-state photophysical properties of the clathrate compounds. The styles of  $\pi$ - $\pi$  stacking between host molecules of the four carboxylic acid inclusion compounds were quite similar to each other; however, a detailed comparison of the crystal structures of the

four carboxylic acid inclusion compounds clarified that the  $\pi$ - $\pi$  interactions between the host molecules decreased with an increase in the size of the enclathrated guest molecules:  $1 \cdot (\text{CH}_3\text{COOH})_2 > 1 \cdot (\text{CH}_3\text{CH}_2\text{COOH})_2 > 1 \cdot [\text{CH}_3\text{CH}_2\text{C}(\text{CH}_2)_2\text{COOH}]_2 > 1 \cdot [\text{HOOC}(\text{CH}_2)_8\text{COOH}]_2$ . These results confirm that the differences in the destruction of the host-host  $\pi$ - $\pi$  interactions by enclathration of the carboxylic acid molecules are reflected on the guest size-dependent fluorescence enhancement. However, the solid-state fluorescence intensity of  $1 \cdot [\text{HOOC}(\text{CH}_2)_8\text{COOH}]_2$  is weaker than that of  $1 \cdot [\text{CH}_3\text{CH}_2\text{C}(\text{CH}_2)_2\text{COOH}]_2$ . It is considered that the continuous intermolecular hydrogen bond ranging alternately host and guest ( $\cdots\text{H}\cdots\text{G}\cdots\text{H}\cdots$ ) was observed only in  $1 \cdot [\text{HOOC}(\text{CH}_2)_8\text{COOH}]_2$ , which is a principal factor leading to fluorescence quenching in the solid state.<sup>[8]</sup> In contrast, on the basis of the absorption and fluorescence spectra of **1** in acetic acid, the semiempirical MO calculations and the X-ray crystal structure of the carboxylic acid inclusion compounds, the protonation of the imidazole ring of host **1** in the carboxylic acid inclusion crystals would contribute to a redshift in the absorption and emission spectra of the crystals because of an increase in intramolecular charge-transfer character of the host fluorophore by strong resonance interaction of the diethylamino group with the protonated imidazole ring.

## Conclusions

We have designed and synthesized a phenanthro[9,10-*d*]imidazole-type fluorescent clathrate host, 2-[4-(diethylamino)phenyl]-1*H*-phenanthro[9,10-*d*]imidazole (**1**), containing an imidazole ring and a diethylamino group. The crystals of **1** exhibit a drastic fluorescence enhancement with a redshift in the emission maximum upon enclathration of various carboxylic acids. The X-ray crystal structures of the guest-free and carboxylic acid inclusion compounds demonstrated that the differences in the destruction of the host-host  $\pi$ - $\pi$  interactions by enclathration of the carboxylic acid molecules are reflected in the guest size-dependent fluorescence enhancement. Furthermore, on the basis of the absorption and fluorescence spectra of **1** in acetic acid, semiempirical MO calculations and X-ray crystal structure of the carboxylic acid inclusion compounds, the protonation of the imidazole ring of host **1** in the carboxylic acid inclusion crystals would contribute to a redshift in the absorption and emission spectra of the crystals because of an increase in the intramolecular charge-transfer character of the host fluorophore by strong resonance interaction of the diethylamino group with the protonated imidazole ring. Our results indicate that fluorescent clathrand **1** can be utilized as a chemical solid sensor for recognition of gaseous carboxylic acids.

## Experimental Section

**General:** Elemental analyses were measured with a Perkin-Elmer 2400 II CHN analyzer. IR spectra were recorded with a JASCO

FT/IR-5300 spectrophotometer for samples in KBr pellet form. Single-crystal X-ray diffraction was performed with a Rigaku AFC7S diffractometer. Absorption spectra were observed with a JASCO U-best30 spectrophotometer, and fluorescence spectra were measured with a JASCO FP-777 spectrophotometer. The fluorescence quantum yields ( $\Phi$ ) were determined with a Hamamatsu C9920-01 equipped with CCD by using a calibrated integrating sphere system ( $\lambda_{\text{ex}} = 363 \text{ nm}$ ). For measurement of the solid-state fluorescence excitation and emission spectra of the crystals, a Jasco FP-1060 attachment was used.  $^1\text{H}$  NMR spectra were recorded with a JNM-LA-400 (400 MHz) FTNMR spectrometer with tetramethylsilane (TMS) as an internal standard.

**2-[4-(Diethylamino)phenyl]-1H-phenanthro[9,10-d]imidazole (1):** A solution of 9,10-phenanthrenequinone (5.00 g, 24.0 mmol), *p*-diethylaminobenzaldehyde (4.26 g, 24.0 mmol) and ammonium acetate (29.6 g, 0.38 mol) in acetic acid (90 mL) was stirred at 110 °C for 3 h. The reaction mixture was poured into ice-cold water. The resulting precipitate was filtered, washed with water and dried. The residue was purified by chromatography on silica gel ( $\text{CH}_2\text{Cl}_2$ /ethyl acetate, 3:1) to give **1** (7.09 g, 81%) as a milk-white powder. M.p. 319–320 °C.  $^1\text{H}$  NMR (400 MHz,  $[\text{D}_6]\text{DMSO}$ , TMS):  $\delta = 1.14$  (t, 6 H), 3.45 (m, 4 H), 6.83 (d,  $J = 7.81 \text{ Hz}$ , 2 H), 7.57–7.72 (m, 4 H), 8.09 (d,  $J = 7.56 \text{ Hz}$ , 2 H), 8.53 (d,  $J = 7.56 \text{ Hz}$ , 2 H), 8.82 (d,  $J = 7.81 \text{ Hz}$ , 2 H) ppm. IR (KBr):  $\tilde{\nu} = 3069, 1611 \text{ cm}^{-1}$ .  $\text{C}_{25}\text{H}_{23}\text{N}_3$  (365.47): calcd. C 82.16, H 6.34, N 11.50; found C 82.45, H 6.09, N 11.62.

**Preparation of Guest-Inclusion Crystals for Measurement of Solid-State Fluorescence Excitation and Emission Spectra:** Host compound **1** was dissolved with heating in the respective guest solvent. The solution was filtered and kept for a few days at room temperature. The crystals that formed were collected by filtration. The host (H)/guest (G) stoichiometric ratio of the inclusion compounds was determined by integration of the signals in the  $^1\text{H}$  NMR spectrum and CHN analysis.

**1 (Guest-free):** Host **1** (500 mg) was dissolved by warming in acetonitrile (600 mL), and the resulting solution was allowed to stand at room temperature. The crystals (milk-white, needle, 420 mg) were collected and dried on the filter paper.

**1·Formic Acid (H/G, 1:2):** Host **1** (300 mg) was dissolved by warming in a mixture of formic acid and acetonitrile (volume ratio of 1:6, 21 mL), and the resulting solution was allowed to stand at room temperature. The crystals (yellow, needle, 382 mg) were collected and dried on the filter paper.

**1·Acetic Acid (H/G, 1:2):** Host **1** (500 mg) was dissolved by warming in a mixture of acetic acid and acetonitrile (volume ratio of 1:3, 10 mL), and the resulting solution was allowed to stand at room temperature. The crystals (yellow, prism, 297 mg) were collected and dried on the filter paper.  $\text{C}_{29}\text{H}_{31}\text{N}_3\text{O}_4$  (485.57): calcd. C 71.73, H 6.43, N 8.65; found C 71.94, H 6.57, N 8.76.

**1·Propionic Acid (H/G, 1:2):** Host **1** (565 mg) was dissolved by warming in a mixture of propionic acid and acetonitrile (volume ratio of 1:1, 20 mL), and the resulting solution was allowed to stand at room temperature. The crystals (yellow, prism, 661 mg) were collected and dried on the filter paper.  $\text{C}_{31}\text{H}_{35}\text{N}_3\text{O}_4$  (513.63): calcd. C 72.49, H 6.87, N 8.18; found C 72.69, H 7.03, N 8.28.

**1·Hexanoic Acid (H/G, 1:2):** Host **1** (300 mg) was dissolved by warming in a mixture of hexanoic acid and acetonitrile (volume ratio of 1:3, 14 mL), and the resulting solution was allowed to stand at room temperature. The crystals (yellow, prism, 412 mg) were collected and dried on the filter paper.

**1·2,2-Dimethyl-*n*-Butyric Acid (H/G, 1:2):** Host **1** (300 mg) was dissolved by warming in a mixture of 2,2-dimethyl-*n*-butyric acid and acetonitrile (volume ratio of 1:1, 30 mL), and the resulting solution was allowed to stand at room temperature. The crystals (yellow, prism, 411 mg) were collected and dried on the filter paper.

**1·3,3-Dimethyl-*n*-butyric Acid (H/G, 1:2):** Host **1** (300 mg) was dissolved by warming in a mixture of 2,2-dimethyl-*n*-butyric acid and acetonitrile (volume ratio of 1:3, 30 mL), and the resulting solution was allowed to stand at room temperature. The crystals (yellow, prism, 477 mg) were collected and dried on the filter paper.

**1·Benzoic Acid (H/G, 1:1):** Host **1** (500 mg) and benzoic acid (1 g) were dissolved by warming in acetonitrile (600 mL), and the resulting solution was allowed to stand at room temperature. The crystals (white, needle, 608 mg) were collected and dried on the filter paper.  $\text{C}_{32}\text{H}_{29}\text{N}_3\text{O}_2$  (487.59): calcd. C 78.82, H 5.99, N 8.62; found C 79.01, H 6.06, N 8.75.

**1·*m*-Dimethylaminobenzoic Acid (H/G, 1:1):** Host **1** (460 mg) and *m*-dimethylaminobenzoic acid (1.25 g) were dissolved by warming in acetonitrile (600 mL), and the resulting solution was allowed to stand at room temperature. The crystals (yellow, needle, 594 mg) were collected and dried on the filter paper.  $\text{C}_{34}\text{H}_{34}\text{N}_4\text{O}_2$  (530.66): calcd. C 76.95, H 6.46, N 10.56; found C 76.83, H 6.57, N 10.56.

**1·Succinic Acid (H/G, 2:1):** Host **1** (400 mg) and succinic acid (188 mg) were dissolved by warming in acetonitrile (400 mL), and the resulting solution was allowed to stand at room temperature. The crystals (yellow, prism, 295 mg) were collected and dried on the filter paper.

**1·Sebacic Acid (H/G, 2:1):** Host **1** (400 mg) and sebacic acid (221 mg) were dissolved by warming in acetonitrile (300 mL), and the resulting solution was allowed to stand at room temperature. The crystals (yellow, prism, 346 mg) were collected and dried on the filter paper.  $\text{C}_{60}\text{H}_{64}\text{N}_6\text{O}_4$  (933.19): calcd. C 77.22, H 6.91, N 9.01; found C 76.92, H 6.97, N 8.82.

**X-ray Crystallographic Studies:** The reflection data were collected at  $23 \pm 1 \text{ }^\circ\text{C}$  with a Rigaku AFC7S four-circle diffractometer by  $2\theta$ - $\omega$  scan technique and by using graphite-monochromated  $\text{Mo-K}\alpha$  ( $\lambda = 0.71069 \text{ \AA}$ ) radiation at 50 kV and 30 mA. In all case, the data were corrected for Lorentz and polarization effects. A correction for secondary extinction was applied. The reflection intensities were monitored by three standard reflections for every 150 reflections. An empirical absorption correction based on azimuthal scans of several reflections was applied. All calculations were performed by using the teXsan<sup>[16]</sup> crystallographic software package of Molecular Structure Corporation. CCDC-740518 (for **1**), -740519 [for **1**· $(\text{CH}_3\text{COOH})_2$ ], -740520 [for **1**· $(\text{CH}_3\text{CH}_2\text{COOH})_2$ ], -740521 [for **1**· $[\text{CH}_3\text{CH}_2\text{C}(\text{CH}_2)_2\text{COOH}]_2$ ] and -740522 [for **1**· $[\text{HOOC}(\text{CH}_2)_8\text{COOH}]_2$ ] contain the supplementary crystallographic data for this paper. These data can be obtained free of charge from The Cambridge Crystallographic Data Centre via [www.ccdc.cam.ac.uk/data\\_request/cif](http://www.ccdc.cam.ac.uk/data_request/cif).

**Crystal of 1:** The transmission factors ranged from 0.96 to 1.00. The crystal structure was solved by direct methods by using SIR92.<sup>[17]</sup> The structures were expanded by using Fourier techniques.<sup>[18]</sup> The non-hydrogen atoms were refined anisotropically. Some hydrogen atoms were refined isotropically; the rest were fixed geometrically and not refined. Crystallographic data:  $\text{C}_{25}\text{H}_{23}\text{N}_3$ ,  $M = 365.48$ , tetragonal,  $a = 20.675(2) \text{ \AA}$ ,  $b = 20.675(2) \text{ \AA}$ ,  $c = 19.151(6) \text{ \AA}$ ,  $U = 8186(2) \text{ \AA}^3$ ,  $\rho_{\text{calcd.}} = 1.186 \text{ g cm}^{-3}$ ,  $T = 296.2 \text{ K}$ , space group  $I4_1/a$  (no.88),  $Z = 16$ ,  $\mu(\text{Mo-K}\alpha) = 0.70 \text{ cm}^{-1}$ , 3834 reflections measured, 3616 unique ( $R_{\text{int}} = 0.073$ ), which were used

in all calculations. The final  $R$  indices [ $I > 2\sigma(I)$ ],  $R_1 = 0.121$ ,  $wR(F^2) = 0.273$ .

**Crystal of 1-(CH<sub>3</sub>COOH)<sub>2</sub>:** The transmission factors ranged from 0.97 to 1.00. The crystal structure was solved by direct methods by using SAPI91.<sup>[19]</sup> The structures were expanded by using Fourier techniques.<sup>[18]</sup> The non-hydrogen atoms were refined anisotropically. Some hydrogen atoms were refined isotropically; the rest were fixed geometrically and not refined. Crystallographic data: C<sub>29</sub>H<sub>31</sub>N<sub>3</sub>O<sub>4</sub>,  $M = 485.58$ , triclinic,  $a = 11.423(1) \text{ \AA}$ ,  $b = 14.126(2) \text{ \AA}$ ,  $c = 8.770(2) \text{ \AA}$ ,  $\alpha = 105.92(1)^\circ$ ,  $\beta = 105.44(1)^\circ$ ,  $\gamma = 83.68(1)^\circ$ ,  $U = 1310.7(4) \text{ \AA}^3$ ,  $\rho_{\text{calcd.}} = 1.230 \text{ g cm}^{-3}$ ,  $T = 296.2 \text{ K}$ , space group  $P\bar{1}$  (no.2),  $Z = 2$ ,  $\mu(\text{Mo-K}\alpha) = 0.83 \text{ cm}^{-1}$ , 4880 reflections measured, 4627 unique ( $R_{\text{int}} = 0.030$ ), which were used in all calculations. The final  $R$  indices [ $I > 2\sigma(I)$ ],  $R_1 = 0.085$ ,  $wR(F^2) = 0.207$ .

**Crystal of 1-(CH<sub>3</sub>CH<sub>2</sub>COOH)<sub>2</sub>:** The transmission factors ranged from 0.99 to 1.00. The crystal structure was solved by direct methods by using SAPI91.<sup>[19]</sup> The structures were expanded by using Fourier techniques.<sup>[18]</sup> The non-hydrogen atoms were refined anisotropically. Some hydrogen atoms were refined isotropically; the rest were fixed geometrically and not refined. Crystallographic data: C<sub>31</sub>H<sub>35</sub>N<sub>3</sub>O<sub>4</sub>,  $M = 513.64$ , triclinic,  $a = 11.712(2) \text{ \AA}$ ,  $b = 13.955(2) \text{ \AA}$ ,  $c = 9.611(2) \text{ \AA}$ ,  $\alpha = 107.03(1)^\circ$ ,  $\beta = 108.59(2)^\circ$ ,  $\gamma = 84.76(1)^\circ$ ,  $U = 1423.6(5) \text{ \AA}^3$ ,  $\rho_{\text{calcd.}} = 1.198 \text{ g cm}^{-3}$ ,  $T = 296.2 \text{ K}$ , space group  $P\bar{1}$  (no.2),  $Z = 2$ ,  $\mu(\text{Mo-K}\alpha) = 0.80 \text{ cm}^{-1}$ , 5272 reflections measured, 5007 unique ( $R_{\text{int}} = 0.012$ ), which were used in all calculations. The final  $R$  indices [ $I > 2\sigma(I)$ ],  $R_1 = 0.073$ ,  $wR(F^2) = 0.193$ .

**Crystal of 1-[CH<sub>3</sub>CH<sub>2</sub>C(CH<sub>2</sub>)<sub>2</sub>COOH]<sub>2</sub>:** The transmission factors ranged from 0.97 to 1.00. The crystal structure was solved by direct methods by using SIR92.<sup>[17]</sup> The structures were expanded by using Fourier techniques.<sup>[18]</sup> The non-hydrogen atoms were refined anisotropically. Some hydrogen atoms were refined isotropically; the rest were fixed geometrically and not refined. Crystallographic data: C<sub>37</sub>H<sub>47</sub>N<sub>3</sub>O<sub>4</sub>,  $M = 597.80$ , orthorhombic,  $a = 22.296(5) \text{ \AA}$ ,  $b = 27.49(1) \text{ \AA}$ ,  $c = 11.342(4) \text{ \AA}$ ,  $U = 6951(2) \text{ \AA}^3$ ,  $\rho_{\text{calcd.}} = 1.141 \text{ g cm}^{-3}$ ,  $T = 296.2 \text{ K}$ , space group  $Pbca$  (no.61),  $Z = 8$ ,  $\mu(\text{Mo-K}\alpha) = 0.74 \text{ cm}^{-1}$ , 6125 reflections measured, 6123 unique ( $R_{\text{int}} = 0.083$ ), which were used in all calculations. The final  $R$  indices [ $I > 2\sigma(I)$ ],  $R_1 = 0.097$ ,  $wR(F^2) = 0.252$ .

**Crystal of 1-[HOOC(CH<sub>2</sub>)<sub>8</sub>COOH]<sub>2</sub>:** The transmission factors ranged from 0.96 to 1.00. The crystal structure was solved by direct methods by using SIR92.<sup>[17]</sup> The structures were expanded by using Fourier techniques.<sup>[18]</sup> The non-hydrogen atoms were refined anisotropically. Some hydrogen atoms were refined isotropically; the rest were fixed geometrically and not refined. Crystallographic data: C<sub>30</sub>H<sub>32</sub>N<sub>3</sub>O<sub>2</sub>,  $M = 466.6$ , monoclinic,  $a = 10.819(4) \text{ \AA}$ ,  $b = 18.650(3) \text{ \AA}$ ,  $c = 13.063(3) \text{ \AA}$ ,  $\beta = 102.89(2)^\circ$ ,  $U = 2569(1) \text{ \AA}^3$ ,  $\rho_{\text{calcd.}} = 1.206 \text{ g cm}^{-3}$ ,  $T = 296.2 \text{ K}$ , space group  $P2_1/c$  (no.14),  $Z = 4$ ,  $\mu(\text{Mo-K}\alpha) = 0.76 \text{ cm}^{-1}$ , 4765 reflections measured, 4514 unique ( $R_{\text{int}} = 0.049$ ), which were used in all calculations. The final  $R$  indices [ $I > 2\sigma(I)$ ],  $R_1 = 0.075$ ,  $wR(F^2) = 0.219$ .

**Computational Methods:** The semiempirical calculations were carried out with the WinMOPAC Ver. 3.9 package (Fujitsu, Chiba, Japan). Geometry calculations in the ground state were made by using the AM1 method.<sup>[15]</sup> All geometries were completely optimized (keyword PRECISE) by the eigenvector following routine (keyword EF). Experimental absorption spectra of the eight compounds were compared with their absorption data by the semiempirical method CNDO/S (intermediate neglect of differential overlap/spectroscopic).<sup>[14]</sup> All CNDO/S calculations were performed by using single excitation full SCF/CI (self-consistent field/configura-

tion interaction), which includes the configuration with one electron excited from any occupied orbital to any unoccupied orbital, where 225 configurations were considered [keyword CI (15 15)].

## Acknowledgments

This work was partially supported by a Grant-in-Aid for Science and Research from the Ministry of Education, Science, Sport and Culture of Japan (Grant 21550181) and by a Special Research Grant for Green Science from Kochi University.

- a) E. Weber, M. Czugler in *Topics in Current Chemistry Vol. 149: Molecular and Molecular Recognition – Clathrates II* (Ed.: E. Weber, Springer, Berlin, **1988**, p. 45; b) E. Weber in *Inclusion Phenomena and Molecular Recognition* (Ed.: J. L. Atwood), Plenum Press, New York, **1990**, vol. 4, p. 188.
- a) H. Langhals, T. Potrawa, H. Nöth, G. Linti, *Angew. Chem. Int. Ed. Engl.* **1989**, *28*, 478–480; b) H. Langhals, R. Ismael, O. Yürük, *Tetrahedron* **2001**, *56*, 5435–5441; c) Z. Fei, N. Kocher, C. J. Mohrschladt, H. Ihmels, D. Stalke, *Angew. Chem. Int. Ed.* **2003**, *42*, 783–787; d) J. L. Scott, T. Yamada, K. Tanaka, *New J. Chem.* **2004**, *28*, 447–450.
- a) F. Toda, *Acc. Chem. Res.* **1995**, *28*, 480–486; b) K. Ochiai, Y. Mazaki, S.-I. Nishikiori, K. Kobayashi, S. Hayashi, *J. Chem. Soc. Perkin Trans. 2* **1996**, 1139–1145.
- a) S. A. Bourne, L. Hohnson, C. Marais, L. R. Nassimbeni, E. Weber, K. Skobridis, F. Toda, *J. Chem. Soc. Perkin Trans. 2* **1991**, 1707–1713; b) I. Csöreg, E. Weber, L. R. Nassimbeni, O. Gallardo, N. Dörpinghaus, A. Ertan, A. A. Bourne, *J. Chem. Soc. Perkin Trans. 2* **1993**, 1775–1782; c) J. D. Wright, *Molecular Crystals*, 2nd ed., Cambridge University Press, New York, **1995**, p. 32.
- a) K. Yoshida, J. Yamazaki, Y. Tagashira, S. Watanabe, *Chem. Lett.* **1996**, 9–10; b) K. Yoshida, T. Tachikawa, J. Yamasaki, S. Watanabe, S. Tokita, *Chem. Lett.* **1996**, 1027–1028; c) Y. Ooyama, K. Yoshida, *New J. Chem.* **2005**, *29*, 1204–1212.
- a) K. Yoshida, H. Miyazaki, Y. Miura, Y. Ooyama, S. Watanabe, *Chem. Lett.* **1999**, 837–838; b) K. Yoshida, Y. Ooyama, S. Tanikawa, S. Watanabe, *Chem. Lett.* **2000**, 714–715; c) K. Yoshida, Y. Ooyama, S. Tanikawa, S. Watanabe, *J. Chem. Soc. Perkin Trans. 2* **2002**, 708–714.
- Y. Ooyama, K. Yoshida, *Eur. J. Org. Chem.* **2008**, *15*, 2564–2570.
- a) Y. Ooyama, S. Nagano, M. Okamura, K. Yoshida, *Eur. J. Org. Chem.* **2008**, *35*, 5899–5906; b) Y. Ooyama, S. Nagano, K. Yoshida, *Tetrahedron* **2009**, *65*, 1467–1474.
- Y. Mizobe, N. Tohnai, M. Miyata, Y. Hasegawa, *Chem. Commun.* **2005**, 1839–1841.
- a) Y. Imai, K. Kawaguchi, T. Harada, T. Sato, M. Ishikawa, M. Fujiki, R. Kuroda, Y. Matsubara, *Tetrahedron Lett.* **2007**, *48*, 2927–2930; b) Y. Imai, K. Murata, K. Kawaguchi, T. Sato, N. Tajima, R. Kuroda, Y. Matsubara, *Chem. Asian J.* **2008**, *3*, 625–629.
- K. Yoshida, K. Uwada, H. Kumaoka, L. Bu, S. Watanabe, *Chem. Lett.* **2001**, 808–809.
- a) B. Metten, M. Smet, N. Boens, W. Dehaen, *Synthesis* **2005**, *11*, 1838–1844; b) F. Wendeborn, B. Schmidhalter, T. Schaefer, P. Murer, K. Bardou, *PCT Int. Appl. WO 2008031743*, **2008**; c) T. Schaefer, P. Murer, F. Wendeborn, B. Schmidhalter, R. Kristina, P. J. Andrea, *PCT Int. Appl. WO 2008119666*, **2008**.
- a) A. K. Mishra, S. K. Dogra, *Bull. Chem. Soc. Jpn.* **1985**, *58*, 3587–3592; b) J. Dey, S. K. Dogra, *J. Phys. Chem.* **1994**, *98*, 3638–3644; c) C. Krishnamoorthy, S. K. Dogra, *J. Org. Chem.* **1999**, *64*, 6566–6574.
- a) J. E. Ridley, M. C. Zerner, *Theor. Chim. Acta* **1973**, *32*, 111–134; b) J. E. Ridley, M. C. Zerner, *Theor. Chim. Acta* **1976**, *42*, 223–236; c) A. D. Bacon, M. C. Zerner, *Theor. Chim. Acta*

- 1979, 53, 21–54; d) H. A. Kurtz, J. J. P. Stewart, D. M. Dieter, *J. Comput. Chem.* **1990**, 11, 82–87.
- [15] M. J. S. Dewar, E. G. Zoebisch, E. F. Healy, J. J. P. Stewart, *J. Am. Chem. Soc.* **1985**, 107, 3902–3909.
- [16] *teXsan: Crystal Structure Analysis Package*, Molecular Structure Corporation **1985** and **1992**.
- [17] A. Altomare, M. C. Burla, M. Camalli, M. Cascarano, C. Giacovazzo, A. Guagliardi, G. Polidori, *J. Appl. Crystallogr.* **1994**, 27, 435.
- [18] DIRDIF94: P. T. Beurskens, G. Admiraal, G. Beurskens, W. P. Bosman, R. de Gelder, R. Israel, J. M. M. Smits, *The DIRIF94 Program System*, Technical Report of the Crystallography Laboratory, University of Nijmegen, The Netherlands, **1994**.
- [19] *Fan Hai-Fu: Structure Analysis Programs with Intelligent Control*, Rigaku Corporation, Tokyo, Japan, **1991**.

Received: July 23, 2009

Published Online: October 20, 2009